

Broadening the photonic bandgap in adiabatic distributed-Bragg-reflectors*

Shailja Sharma[†], Abhishek Mondal[†] and Ritwick Das[‡]

(Dated: January 11, 2022)

Adiabatic following has been an widely-employed technique for achieving near-complete population transfer in a ‘two-level’ quantum mechanical system. The theoretical basis, however, could be generalized to a broad class of systems exhibiting $SU(2)$ symmetry. In the present work, we present an analogy of population transfer dynamics of two level system with that of light propagation in a classical ‘one-dimensional’ photonic crystal, commonly known as distributed-Bragg-reflector (DBR). This formalism facilitates in adapting the idea of adiabatic following, more precisely the rapid adiabatic passage (RAP) which is usually encountered in a broad class of quantum-mechanical systems. We present two different DBR configurations in which the adiabatic constraints are obeyed along the DBR length by virtue of optimum design. The reflection spectrum for both the configurations exhibit broadening of photonic bandgap (PBG) in addition to a varying degree of suppression of sharp transmission resonances. The intermodal coupling between counter-propagating modes as well as their phase-mismatch, for both the DBR configuration, exhibits a longitudinal variation which is usually observed in ‘Allen-Eberly’ scheme of adiabatic population transfer in *two-level* atomic systems.

I. INTRODUCTION

The propagation characteristics of electromagnetic (*em*) waves in a periodically stratified dielectric medium closely resemble the features exhibited by the matter waves in crystalline solids [1, 2]. In crystals, the periodic *Coulomb*-potential leads to formation of continuous energy bands separated by forbidden energy spectrum, also known as bandgaps. In resemblance, analogous periodic photonic architectures, commonly termed as *photonic crystals* (PCs), lead to formation of *em* transmission *bands* enclosed by forbidden frequency spectrum known as photonic bandgap (PBG) [3, 4]. Over the last four decades, PCs has evolved as backbone of many technological advancements which essentially hinge upon manipulating the spatial and spectral characteristics of light beam [5]. In one-dimension, the PCs are also known as distributed-Bragg-reflector (DBR) and they have turned out to be primary ingredients for devising reflectors/anti-reflectors, spectral and spatial filtering elements and creating efficient sensing platforms which include those involving plasmonic interactions [6–11]. Bragg reflection based waveguiding configurations have been employed as polarization selection device in miniaturized optical sources [12, 13]. Bragg-reflection-waveguides (BRWs) with a vacuum core have been forecasted as plausible hosts for future optical particle accelerators driven by extremely high power lasers [14]. On the other hand,

the possibility of field confinement and therefore, reducing the *em* interaction volume to sub-wavelength scale has lead to the formation of stable spatial-solitons in nonlinear BRWs [15]. Recently, the bulk modes of a BRWs or optical surface states in DBR have been found to be promising candidates for optical parametric processes and higher harmonic generation [16–18]. As mentioned before, a DBR is primarily characterized by PBG whose magnitude is primarily dictated by the refractive index contrast of the DBR constituents and the location in a spectral band is governed by the thickness of constituent layers [5]. Therefore, for a given pair of material forming the DBR, the magnitude of PBG is unique and fixed. Within the limit of optical transparency for the constituent DBR materials, we present a formalism to broaden the PBG (and suppress the transmission band) by utilizing the concept of adiabatic coupling to a backward propagating mode from a forward propagating mode. Therefore, we draw an equivalence of the coupled-wave equations in a DBR with that encountered while describing the dynamics of quantum *two-level* atomic systems. Subsequently, we propose plausible DBR configurations for adopting the adiabatic following in such systems which leads to broadening of PBG spectrum. The formalism could be translated to any spectral band and PBG broadening is limited by the restriction imposed by material transparency only. Interestingly, this idea provides an viable platform to tailor the backscattered phase from such systems as well.

Adiabatic following, also known as rapid adiabatic passage (RAP) has been an well-established technique for realizing near 100% population transfer in a *two-level* atomic systems using optimum ultrashort (≤ 0.5 ps) pulses [19]. In fact, it is quite straightforward to ascertain that the RAP mechanism could be adopted in any equivalent system exhibiting *special unitary*(2) or $SU(2)$ symmetry. For example, RAP provides an efficient platform for ultrashort pulse frequency conversion as well as

* S.S. and A.M. acknowledges the Department of Atomic Energy, Government of India and University Grant Commission, India respectively for financial support. The research is supported by the Science and Engineering Research Board, Government of India, Grant no. CRG/2020/000982.

[†] Both the author has equal contribution.

[‡] School of Physical Sciences, National Institute of Science Education and Research, HBNI, Jatni - 752050, Odisha, India; ritwick.das@niser.ac.in

tailoring spatial characteristics of optical beams in optical nonlinear medium [20–23].

II. ADIABATIC-FOLLOWING IN DBR

A periodic variation (with periodicity Λ) in dielectric constant (ϵ) along z -direction in a medium could be expressed as [24]

$$\epsilon(x, y, z) = \epsilon(x, y) + \Delta\epsilon(x, y, z) \quad (1)$$

where $\Delta\epsilon(x, y, z)$ defines the periodic modulation along z . This dielectric perturbation gives rise to the possibility of intermodal interactions. Let us consider any two modes, namely $|p\rangle$ and $|q\rangle$ propagating through the medium described by dielectric function in Eq. (1). Assuming the modes are propagating along z -direction, the em -field corresponding to the modes (in the paraxial limit) are given by $|p\rangle = E_p(x, y)A_p(z)e^{i(\omega t - \beta_p z)}$ and $|q\rangle = E_q(x, y)A_q(z)e^{i(\omega t - \beta_q z)}$. Under the slowly varying approximation, the evolution of z -dependent mode-amplitude (A_p) of the p^{th} -mode due to the presence of q^{th} -mode (with amplitude A_q) is given by [24]

$$\frac{dA_q}{dz} = -i \frac{\beta_q}{|\beta_q|} \sum_p \sum_m \kappa_{pq}^{(m)} A_p e^{-i(\beta_p - \beta_q - m \frac{2\pi}{\Lambda})z} \quad (2)$$

where β_p and β_q are the normal components of wavevector k_p and k_q respectively. $\kappa_{pq}^{(m)}$ defines the magnitude of coupling coefficient which couples the modes through the m^{th} Fourier component of dielectric function Eq. (1). The m^{th} coupling coefficient is expressed as

$$\kappa_{pq}^{(m)} = \frac{\omega}{4} \int \int E_p^*(x, y) \epsilon_m(x, y) E_q(x, y) dx dy \quad (3)$$

where ϵ_m is the m^{th} component of Fourier-series expansion of ϵ (see Eq. 1). The coupling between the interacting modes is maximum when the longitudinal phase-matching condition is exactly satisfied,

$$\beta_p - \beta_q - m \frac{2\pi}{\Lambda} = 0 \quad (4)$$

In case of DBR, the coupling between a forward propagating mode ($A_p \equiv A_i$) and a backward propagating mode ($A_q \equiv A_r$) is of interest. In absence of any other intermodal interactions, the forward-backward mode coupling (assuming $m = 1$) would be governed by [24–26],

$$\frac{dA_r}{dz} = -i \frac{\beta_r}{|\beta_r|} \kappa A_i e^{i\Delta\beta z} \quad (5)$$

$$\frac{dA_i}{dz} = -i \frac{\beta_i}{|\beta_i|} \kappa^* A_r e^{-i\Delta\beta z} \quad (6)$$

where we have dropped the indices from κ and $\Delta\beta = \beta_r - \beta_i - \frac{2\pi}{\Lambda}$. In case the DBR constituent materials are isotropic, the dielectric function (Eq. (1)) is a

purely scalar and consequently, transverse-electric (TE) to transverse-magnetic (TM) mode-coupling (and vice-versa) is forbidden. It is worth noting that the phase-matching condition for coupling $|i\rangle$ to $|r\rangle$ (or $|r\rangle$ to $|i\rangle$) coupling is contra-directional in nature and could be expressed as $\Delta\beta = 2\beta - \frac{2\pi}{\Lambda} = 0$ where $\beta_i = -\beta_r = \beta$ [24]. As shown in Fig.1 below, in case of an oblique incidence of optical beam (θ with respect to z -axis), the phase-matching condition for the contra-directional coupling process is modified to $\Delta\beta = 2\beta \cos\theta - \frac{2\pi}{\Lambda} = 0$. For a simple case when the two layers of the DBR (with refractive indices n_1 and n_2) share the same thickness *i.e.* $d_1 = d_2$, the coupling coefficient takes a simplified form given by [24],

$$\kappa_{TE} = \frac{i}{\lambda \cos\theta} \frac{\sqrt{2}(n_1^2 - n_2^2)}{\sqrt{(n_2^2 + n_1^2)}} \quad (7)$$

$$\kappa_{TM} = \frac{i}{\lambda \cos\theta} \frac{\sqrt{2}(n_1^2 - n_2^2)}{\sqrt{(n_2^2 + n_1^2)}} \cos 2\theta \quad (8)$$

The solution of Eqs. (5) and (6) in a perfectly phase-matched ($\Delta\beta = 0$) situation leads to a strong coupling from $|i\rangle$ to $|r\rangle$ for broad range of frequencies situated within the PBG and consequently, we obtain a strong reflection band. It is apparent from Eq. (7) (or (8)) that the contrast in refractive index (or dielectric constant) is the primary factor determining the strength of coupling. For a given choice of DBR constituents, $|n_1^2 - n_2^2|$ is fixed and consequently, the width of PBG remains unchanged.

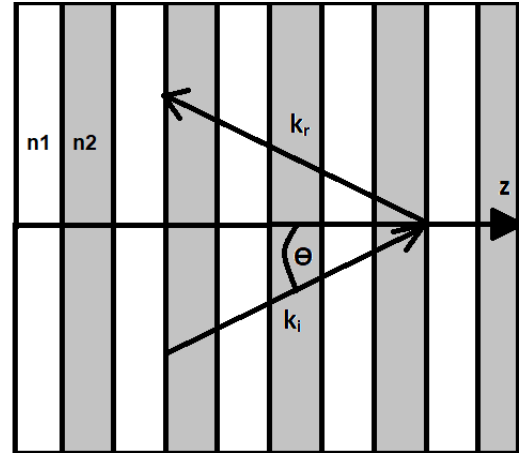


FIG. 1. Oblique incidence of em -wave on distributed-Bragg-reflector (DBR). z -direction represents the optical axis

A. Adiabatic phase-matching

We consider the following transformation to a rotating frame given by

$$A_r = \tilde{a}_r e^{i/2[\Delta\beta(0)z - \int_0^z q(\tilde{z})d\tilde{z}]} \quad (9)$$

$$A_i = \tilde{a}_i e^{-i/2[\Delta\beta(0)z - \int_0^z q(\tilde{z})d\tilde{z}]} \quad (10)$$

where $\Delta\beta(0)$ is the phase-mismatch at $z = 0$, $q(z)$ is determined by the dielectric constant modulation $\Delta\epsilon$ (as per Eq. (1)), and $\Delta k = \frac{\Delta\beta(0) - q(z)}{2}$. The substitution of Eqs. (9) and (10) into Eqs. (5) and (6) yields

$$i \frac{d}{dz} \begin{pmatrix} \tilde{a}_i \\ \tilde{a}_r \end{pmatrix} = \begin{pmatrix} -\Delta k & \kappa \\ -\kappa^* & \Delta k \end{pmatrix} \begin{pmatrix} \tilde{a}_i \\ \tilde{a}_r \end{pmatrix} \quad (11)$$

which is an equivalent representation of time-dependent Schrödinger equation in optics. In fact, if we define a state $|\Psi\rangle = \begin{pmatrix} \tilde{a}_i \\ \tilde{a}_r \end{pmatrix}$ then $-i \frac{d}{dz} |\Psi\rangle = \hat{H} |\Psi\rangle$ where time-dependence is replaced by the z -dependence and the Hamiltonian $\hat{H} = \vec{\sigma} \cdot \vec{B}$. Here, $\vec{\sigma} = (\sigma_x, \sigma_y, \sigma_z)$ are the Pauli-spin matrices and $\vec{B} = (\kappa, 0, -\Delta k)$ represents a fictitious magnetic field. The Hamiltonian has a close resemblance with that representing the dynamics of a spin-1/2 particle in an external magnetic field where $|i\rangle$, $|r\rangle$ are the equivalent to the spin-up ($|\uparrow\rangle$) and spin-down ($|\downarrow\rangle$) states[27]. In order to represent a particular spin-state, the equivalent Stokes parameters could be given by $S_j = \langle \sigma_j \rangle$ ($j \equiv x, y, z$) and the evolution of the state would be dictated by $\frac{\partial S_j}{\partial z} = -i \langle [\sigma_j, \hat{H}] \rangle$. This, subsequently, leads to

$$\begin{aligned} S_x &= \tilde{a}_i \tilde{a}_r^* + \tilde{a}_r \tilde{a}_i^* \\ S_y &= -i[\tilde{a}_i \tilde{a}_r^* - \tilde{a}_r \tilde{a}_i^*] \\ S_z &= |\tilde{a}_i|^2 - |\tilde{a}_r|^2 \end{aligned} \quad (12)$$

and

$$\dot{\vec{S}} = \vec{B} \times \vec{S} \quad (13)$$

where $\dot{\vec{S}} \equiv \frac{\partial \vec{S}}{\partial z}$. The states and their evolution described by Eqs. ((12)) and ((13)) could be mapped onto an equivalent Bloch-sphere where $|i\rangle$ (spin-up) and $|r\rangle$ (spin-down) states are located the *north*-pole and *south*-pole respectively. The fictitious magnetic-field (\vec{B}) results in a *torque* on the system which leads to precession of the state vector (\vec{S}) about \vec{B} with a frequency $|\vec{B}| = \sqrt{|\kappa|^2 + \Delta k^2}$. It is worthwhile to point out that the value S_z (Eq. (12)) determines the mode-conversion (from the forward-to-backward or vice-versa) factor. The state $\vec{S} = [0, 0, 1]$ represents a situation where the incident beam contains all the optical power *i.e.* $\tilde{a}_i = 1$ and the state $\vec{S} = [0, 0, -1]$ represents the case when all the optical power is present in the reflected beam ($\tilde{a}_r = 1$). The coupling efficiency to the reflected beam is expressed as $\eta = \frac{S_z + 1}{2}$. The dynamics, here, is primarily controlled by Δk and κ which are essentially equivalent to factors *detuning* (Δ) and *Rabi-frequency* (Ω) respectively which are commonly encountered in a *two-level* atomic system. In perfectly phase-matched case ($\Delta k = 0$), which is satisfied for the central PBG frequency, a gradual semi-circular rotation of the state-vector (\vec{S}) from north-pole

to the south-pole takes place on DBR Bloch-sphere which implies a complete transfer of optical power from the incident beam to the reflected beam in the DBR. In order not to obscure the salient features of the equivalent dynamics, we have ignored the role played by absorption loss (α) in the dielectric materials. However, it would be worthwhile to point out that the role of absorption loss is equivalent to that played by semi-phenomenological decay constant (T_2) in a *two-level* atomic system [19]. For $\Delta k \neq 0$, \vec{S} traces a trajectory on the DBR Bloch-sphere about the axis $\hat{n} = \frac{\kappa \hat{x} + \Delta k \hat{z}}{\sqrt{\kappa^2 + \Delta k^2}}$. This implies that $\Delta k \neq 0$ leads to transportation of state-vector \vec{S} to a point in southern-hemisphere. This point may be near the south-pole but it will never be the south-pole of the equivalent DBR Bloch-sphere. Nevertheless, S_z still negative and the reflectivity is large (not maximum). The frequencies for which S_z remains negative forms a band of frequencies constituting the PBG. However, a sufficiently large Δk results in a \hat{n} such that \vec{S} is transported to a point which lies on the northern hemisphere of DBR Bloch-sphere (assuming \vec{S} starts precessing about \vec{B} from north-pole). Therefore, S_z would be positive after propagation through the DBR. This corresponds to frequencies outside the PBG (or within the transmission band) where reflectivity is much smaller than the PBG. In fact, the *equator* of DBR Bloch-sphere distinguishes the PBG (southern hemisphere) from the transmission (pass) band (northern hemisphere) with respect to the trajectory of \vec{S} .

It is apparent that $\Delta k = 0$ along the entire DBR length for the central PBG frequency and $\Delta k \neq 0$ for all other frequencies. The aforementioned analogy to a *two-level* atomic system, thus, allows us to adopt the Rapid Adiabatic Passage (RAP) mechanism for broadening the PBG spectrum and suppressing the transmission (pass) bands in the DBR. Consequently, we propose DBR configurations which leads to *slow* variation in Δk from a large negative to a large positive value along the DBR length such that the sweep always remains much smaller than the coupling (κ). This would ensure nearly complete transfer of optical power from a forward propagating to a backward propagating mode across a frequency band extending much beyond the conventional PBG of a DBR. The RAP condition is expressed as [19, 28]

$$\kappa \dot{\Delta k} - \Delta k \dot{\kappa} \ll (|\kappa|^2 + \Delta k^2)^{3/2} \quad (14)$$

which essentially implies that the *rate* of change of polar angle $\Phi = \tan^{-1}(\frac{\kappa}{\Delta k})$ (angle between \vec{B} and z axis) during the evolution is much slower with the frequency of rotation ($= \sqrt{\kappa^2 + \Delta k^2}$) for \vec{S} about \vec{B} . If κ is assumed to be constant (along z), the adiabaticity condition appears as $\frac{d\Delta k}{dz} \ll \frac{(\kappa^2 + \Delta k^2)^{3/2}}{\kappa}$. Also, in order to achieve near-complete optical power transfer, it is essential that the two states $|i\rangle$ and $|r\rangle$ are decoupled at the entry ($z = -\frac{L}{2}$) and exit ($z = +\frac{L}{2}$) faces of the DBR. Alternately, this is mathematically expressed as $|\frac{\Delta\beta}{\kappa}| \gg 2$

at $z = \pm \frac{L}{2}$ which is equivalent to satisfying the condition of *autoresonance* in ‘two-wave’ interaction system [29, 30]. In this case, *autoresonance* essentially ensures that the counter-propagating modes remain phase-locked when the parameters of the Hamiltonian undergo an adiabatic change and consequently, near-complete transfer of optical power.

B. DBR configurations for adiabatic mode-conversion

1. Intra-cell boundary tilt

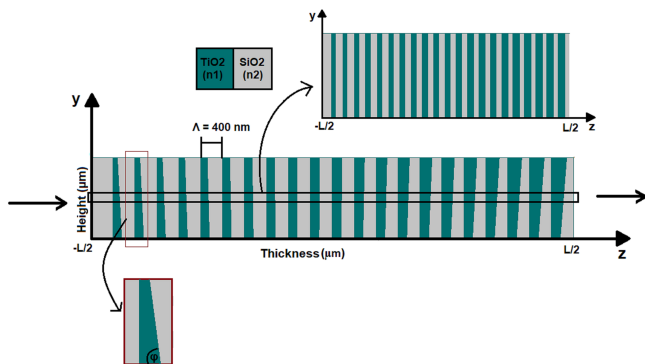


FIG. 2. A schematic for intra-cell tilt (ICT) DBR where the interface between TiO_2 (A) and SiO_2 (B) layer (within a unit cell) is tilted along z -direction. The tilt angle (θ) linearly and symmetrically reduces from one-end to the other end of the DBR.

We consider a DBR shown in Fig. 2 where a unit cell is comprised of two layers, namely A (TiO_2) and B (SiO_2). The intra-cell tilt (ICT) angle defining the boundary between A and B gradually changes in each unit cell. The unit cell thickness boundary, however, remains normal to z -axis as shown in Fig. 2. The ICT angle ($\theta = 90^\circ - \phi$) in the M^{th} unit cell is given by

$$\cot \theta = \frac{h}{(d_1/2) - (M-1)l} \quad (15)$$

where h represents the transverse extent (along y) of the geometry, l is the change in thickness of layer A at $y = h$ in the M^{th} unit cell, $d_1 = 200 \text{ nm}$ is the unperturbed thickness of layer A and $0 \leq \theta \leq \frac{\pi}{2}$. The variation in θ along the propagation direction (as a function of M) is shown in Fig. 3(a). For such a DBR geometry, κ (defined in Eq. (3)) changes marginally across the DBR length. However, the phase-mismatch Δk ($= \frac{\Delta\beta}{2}$) is a function of θ which is expressed as

$$\Delta\beta(\theta) = 2\beta \cos \theta - \frac{2\pi}{\Lambda} \quad (16)$$

Equation (16) yields a variation in Δk shown in Fig. 3 (a) for θ varying from -0.5° to $+0.5^\circ$. Δk monotonically increases from a negative (at $z = -\frac{L}{2}$) to a positive value (at $z = 0$) for the geometry shown in Fig. 2. In the 2^{nd} half of the crystal, Δk takes an identical negative value after traversing through a symmetric path. The variation in $\frac{\partial \Delta k}{\partial z}$ is shown in Fig. 3(b) which ensures that the RAP condition given by the Eq. (14) is satisfied across the ICT DBR length. Once the condition for RAP is satisfied, we explore the possibility of satisfying the auto-resonant condition across the ICT-DBR length [29]. The auto-resonant condition is given by *i.e.* $|\frac{\Delta\beta}{\kappa}| \leq 2$ which essentially implies that the counter-propagating mode at any frequency would be phase-locked in the entire interaction region if it is phase-matched ($\Delta\beta = 0$) to a forward propagating mode in any one *unit cell*. From Fig. 3(c), this condition is satisfied along the entire ICT-DBR length which further strengthens the possibility of PBG enhancement.

In order to simulate the *em*-wave propagation through the ICT DBR geometry, we consider a $4 \mu\text{m} \times 4 \mu\text{m}$ cross-section of the ICT DBR as shown in the zoomed-out section in Fig. 2. A broadband plane-wave is incident on the ICT DBR from region $z < 0$. The reflection spectrum was obtained using finite element method (FEM) (wave-optics module, COMSOL Multiphysics) where $N = 21$ is considered for the present case. The periodic boundary condition is imposed along the transverse direction and a mesh-size of 5 nm is considered for the simulation. Also, we ignore the material dispersion in the present case and assumed $n_1 = 2.5$ ($A \equiv TiO_2$) and $n_2 = 1.5$ ($B \equiv SiO_2$) across the entire spectrum. The ICT-DBR reflection spectrum (when θ varies from -0.05° to $+0.05^\circ$) for normal incidence is shown in Fig. 3(d). If we define PBG to be the difference between wavelengths (frequencies) where the reflectivity (\mathbf{R}) drops by 90% (with respect to the maximum), then the ICT-DBR exhibits an $\approx 90 \text{ nm}$ enhancement in PBG with respect to the normal DBR ($\Lambda = 400 \text{ nm}$). It is interesting to note that the reflection spectrum is marked by suppression of transmission resonances on higher frequency regime ($\geq 215 \text{ THz}$). This could be understood by noting the fact that the frequencies in *high-reflection* band (defined for $\mathbf{R} \geq 90\%$) exhibit an adiabatic transport of the state-vector (\vec{S}) from the north-pole to points on the southern-hemisphere of DBR Bloch-sphere when Δk is slowly swept along the z -direction. In order to have a unity transmission (pass band) *i.e.* complete back-conversion from $|r\rangle$ to $|i\rangle$, \vec{S} must return to the north-pole for that frequency. The variation in Δk (or $\Delta\beta$), in case of ICT-DBR allows return to the northern hemisphere of DBR Bloch-sphere but not necessarily the north-pole. Consequently, the transmission for such frequencies (where a transmission peak is expected) is smaller. From an alternate perspective, ICT-DBR arrangement provides a favourable platform for constructive interference amongst the backward propagating waves over a broader (with respect to normal DBR) spectral band which, in turn leads to drop in

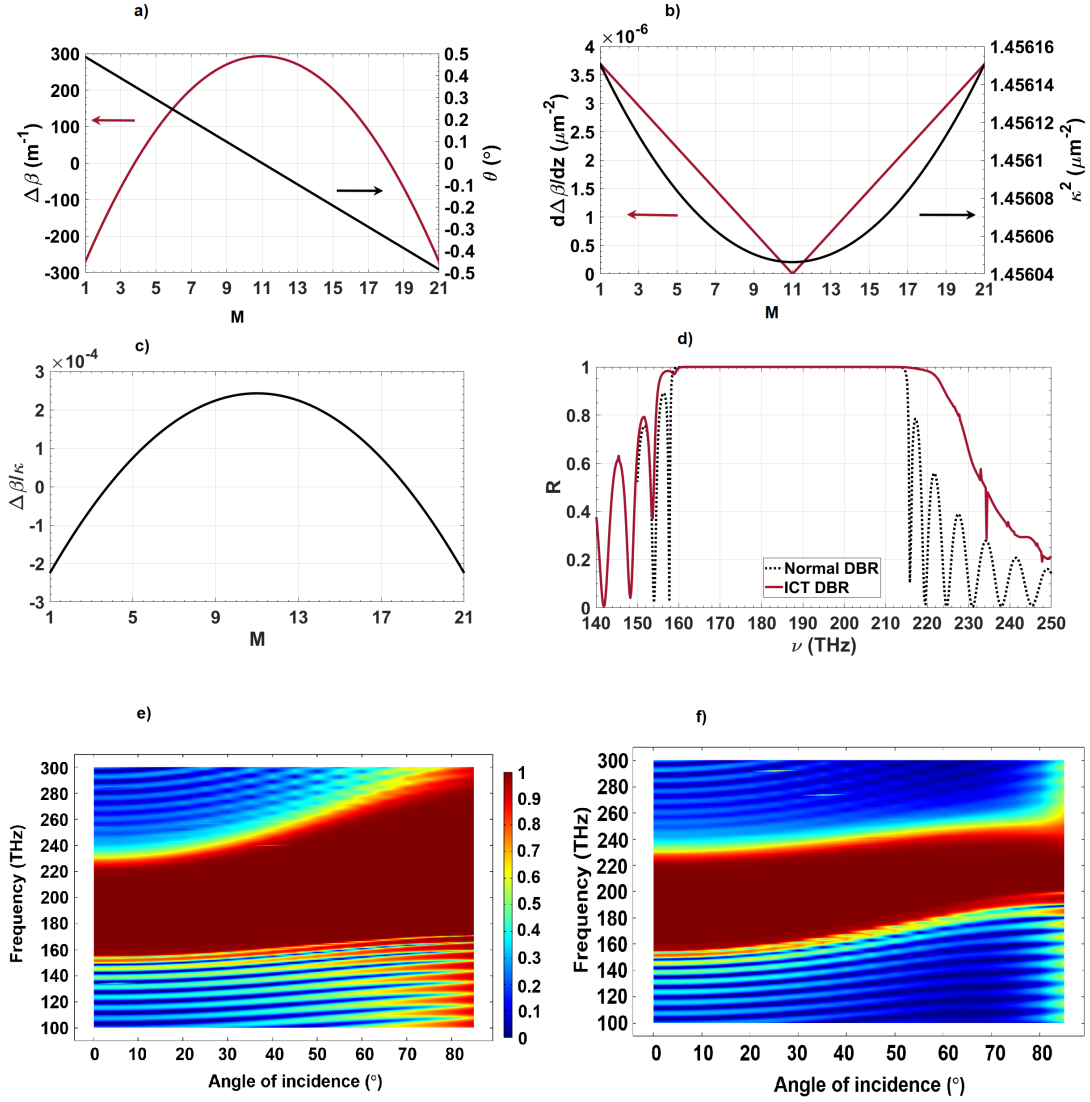


FIG. 3. a) Shows the value of tilt angle θ in each unit cell along with the variation of longitudinal phase-mismatch $(\Delta\beta) = 2\Delta k$ in each (or M^{th}) unit cell of ICT-DBR. b) shows the variation of $\frac{d\Delta\beta}{dz}$ and $|\kappa^2|$ as a function of unit cell number M c) shows the variation of the ratio $|\frac{\Delta\beta}{\kappa}|$ in the M^{th} unit cell of ICT-DBR. d) Reflection spectrum for normal incidence on a normal-DBR (dotted line) and a ICT-DBR with (solid line) when the intra-cell tilt angle $\theta = 0.05^\circ$. e) & f) Reflection spectrum of ICT-DBR as a function of angle of incidence for TE and TM polarization respectively.

transmission for frequencies outside the PBG.

The angle-dependent reflection spectrum for the transverse-electric (TE) polarization of the ICT-DBR has been plotted in Figs. 3(e) and (f). Although, the ICT-DBR reflection spectrum exhibits a similar angular dependence to that exhibited by normal-DBR, the changes in the PBG for TE and TM polarization exhibit a significantly different scaling in comparison with the normal-DBR. The reflection spectrum is simultaneously marked by strong suppression of transmission resonances (for both TE and TM) at higher angles of incidence.

It is worth pointing out that a wider variation of θ (say from -1° to $+1^\circ$) would lead to further broadening of PBG and corresponding suppression of transmission

resonances. However, this is accompanied by unavoidable resonances within the PBG which share features identical to the defect-induced local field confinement. This is expected if we note that the cumulative optical phase-shift due to tilting the intra-cell boundaries could support a *defect-like* mode. The signature of such a cumulative impact manifests as reflectivity drop (resonance) for certain frequencies within the PBG. It is important to note that the value of κ (defined in Eqs.((7) and ((8))) remains almost same along the entire ICT-DBR length. Therefore, the forward and backward propagating modes in the ICT-DBR are not completely decoupled (*i.e.* $|\Delta\beta| \gg \kappa$) at $z = -\frac{L}{2}$ and $z = +\frac{L}{2}$. Consequently, the adiabaticity condition is partially satisfied in case of ICT-DBR. Its

impact could be observed in the form of strong transmission resonances in the low frequency ($\leq 160 THz$) PBG-edge of ICT-DBR (see Fig. 3d).

2. Chirped DBR

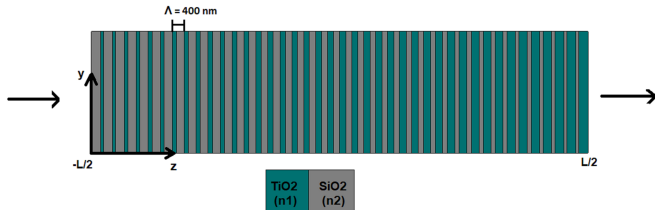


FIG. 4. A schematic to describe the geometry of a chirped-DBR

We consider a DBR configuration with a linear chirp in the duty cycle of each unit cell *i.e.* thickness $d_{1M} = d_1 + M\delta$ and $d_{2M} = \Lambda - d_1 - M\delta$ define the thickness of layers *A* and *B* respectively in M^{th} unit cell. The unit cell period (Λ), however remains unchanged. Here, $M = 0, 1, 2, 3, \dots, (N - 1)$ where N is the total number of unit cells in the DBR. This leads to a longitudinal variation in Δk through a monotonic change in average refractive index of an *unit cell* which could be defined as $\bar{n} = \sqrt{\frac{d_{1M}n_1^2 + d_{2M}n_2^2}{\Lambda}}$. It is worthwhile to note that the variation of \bar{n} also manifests in the form z -dependence of κ . Using Eqs. ((4)), ((7)) and ((8)), the variation in Δk and κ for normal incidence ($\theta = 0$) would be expressed as [24]

$$\Delta k = \frac{\Delta\beta}{2} = \frac{2\pi\bar{n}}{\lambda} - \frac{\pi}{\Lambda} \quad (17)$$

$$\kappa = \frac{i(1 - \cos(\frac{2\pi d_{1M}}{\Lambda})) (n_1^2 - n_2^2)}{2\lambda \bar{n}} \quad (18)$$

For an arbitrarily chosen chirp-length of $\delta = 10 nm$, $d_1 = 10 nm$ and $N = 39$, the variation in Δk and κ for the chirped-DBR (C-DBR) is shown in Fig. 4(a). It is apparent that $\Delta\beta (= 2\Delta k)$ varies symmetrically from a large negative (at $z = -\frac{L}{2}$ or $M = 0$) to a large positive value (at $z = +\frac{L}{2}$ or $M = 38$). The coupling coefficient (κ), on the other hand, reaches a maximum at the center of C-DBR geometry ($M = 20$) and negligibly small at $z = \pm\frac{L}{2}$. Figure 4(b) shows the variation of $\kappa \frac{d\Delta\beta}{dz} - \Delta\beta \frac{d\kappa}{dz}$ in M^{th} unit cell of C-DBR. It is apparent that this is much smaller than $(\kappa^2 + \Delta\beta^2)^{3/2}$ at any point within the C-DBR. Therefore, the adiabaticity condition described by Eq. (14) is completely satisfied in case of C-DBR. It is interesting to note that the auto-resonant condition *i.e.* $|\frac{\Delta\beta}{\kappa}| < 2$ is satisfied in a significant fraction of the C-DBR ($M \approx 10$ to $M \approx 28$) as shown in Fig. 4(c). This essentially implies that the counter-propagating modes

would be phase-locked in the entire interaction region if they are phase-matched ($\Delta\beta = 0$) in any one *unit cell* of C-DBR. The adiabaticity condition has profound impact on reflection spectrum shown in Fig. 4(d). In order to compare, the reflection spectrum for a normal DBR (with $\Lambda = 400 nm$) is also shown in the same figure. It is evident that there is $\approx 240 nm$ increase in PBG for C-DBR as compared to the normal DBR. Also, the reflectivity drop at the band-edges is relatively smooth with complete suppression of transmission resonances. In fact, any alteration in geometric parameters has an impact $\Delta\beta$ and κ and consequently, the adiabatic constraints are partially disobeyed. This is expected to reduce the PBG in reflection spectrum along with appearance of sharp transmission resonance (outside PBG). For example, when the chirp-length changes to $\delta = 5 nm$ with $d_1 = 100 nm$ and $N = 39$, the reflection spectrum is shown in Figs. 4(e) where the PBG shrinks to $\approx 182 nm$. It is also worth noting that the reflection spectrum is accompanied by oscillating side-bands with sharp transmission resonances on both ends of the PBG. On reducing the chirp length further to $\delta = 2.5 nm$ ($d_1 = 150 nm$ and $N = 39$), PBG for the C-DBR shrinks to $100 nm$ and discernibly sharper transmission resonances on both ends of PBG which is similar to that exhibited by normal DBR. The underlying cause behind this observation could be traced to the variation of κ (see Eq. (18)). By reducing the chirp length (without changing the DBR length L), the minimum value of κ (at $z = -\frac{L}{2}$) and $z = +\frac{L}{2}$) increases. Therefore, the forward and backward propagating modes are not completely decoupled at the ends of C-DBR when $\delta = 5 nm$ and $\delta = 2.5 nm$. However, reducing the chirp has a weak impact on $\frac{d\Delta\beta}{dz}$. Overall, adiabaticity conditions are partially satisfied for smaller chirp length and consequently, a smaller PBG.

A detailed comparison of reflection spectrum and dispersion for a normal DBR and a C-DBR (with $\delta = 10 nm$) is elucidated in Figs. 6(a)-(d). The dependence of reflection spectrum on angle-of-incidence (AOI) for TE and TM polarization in a normal-DBR is shown in Figs. 6(a) and (b) respectively. The oblique incidence essentially leads to a smaller value of normal component of the wavevector and consequently, the PBGs shift to higher frequencies with increasing AOI. As expected, the PBGs tend to broaden for the TE polarization on oblique incidence. On the other hand, the low frequency PBGs for TM polarization tends to reduce up to an AOI $\approx 60^\circ$ and increases thereafter. The drop in PBG for TM polarization is essentially due to the Brewster's effect at the interface of high and low-index layers. Figures 6(c) and (d) represent the reflection spectrum for the TE and TM polarization respectively for C-DBR. A comparison between Fig. 6(a) and (c) reveals that the C-DBR exhibits appreciably broad PBGs with very narrow transmission bands separating them. At oblique incidence, the PBG in C-DBR broadens further and shifts to higher frequencies.

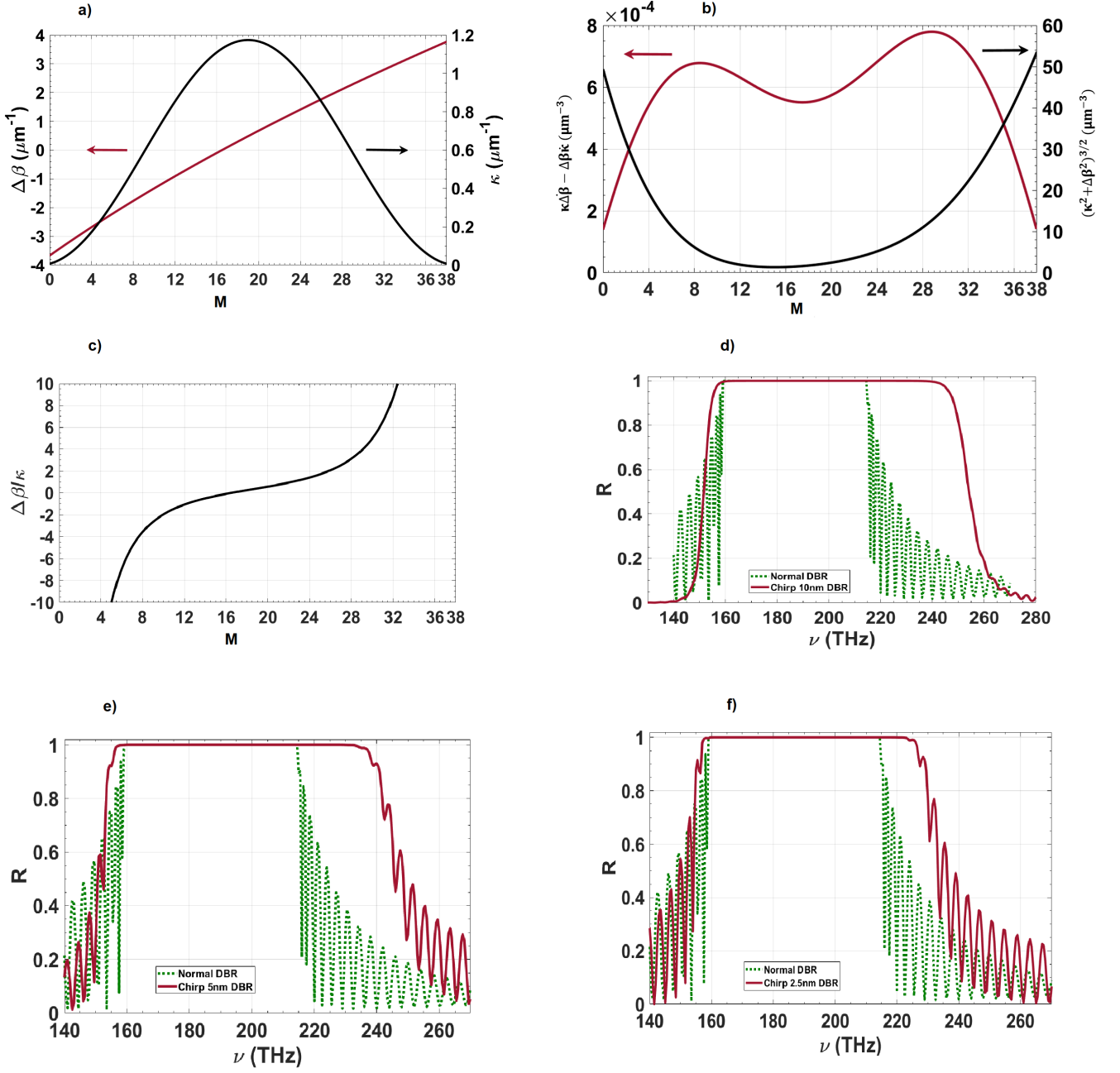


FIG. 5. a) shows the variation of $\Delta\beta$ and κ in M^{th} unit cell. b) shows the variation of LHS and RHS of the inequality given in Eq. 14 in M^{th} unit cell. c) shows the variation of $\frac{\Delta\beta}{\kappa}$ as a function of unit cell no. (M) for depicting a significant fraction of DBR length satisfies the (*condition for auto-resonance*). d), e) and f) shows a comparison between the reflection spectrum of a normal-DBR (dashed green line) of $d_1 = d_2 = 200 \text{ nm}$ with that for C-DBRs (solid red line) having $\delta = 10 \text{ nm}$, $\delta = 5 \text{ nm}$ & $\delta = 2.5 \text{ nm}$ respectively.

This is accompanied by shrinking of transmission bands. In fact, the PBGs tend to overlap for $\text{AOI} \geq 50^\circ$, thereby leading to a high-reflection band extending from 150 THz to 750 THz (1600 nm band). Such broad PBGs are usually not found in normal DBR, even with very wide refractive index contrast. It is also interesting to note that the reflection spectrum (in Fig. 6(c)) exhibits three om-

nidirectional PBGs which are located in $160 - 250 \text{ THz}$, $310 - 400 \text{ THz}$ and $490 - 550 \text{ THz}$ frequency range. The PBG, in this case (for normal as well as oblique incidence) is limited by the material transparency window and could be extended further (on both spectral ends) through suitable choice of materials. A similar comparison between Figs. 6(b) and (d) depict broadened PBG in

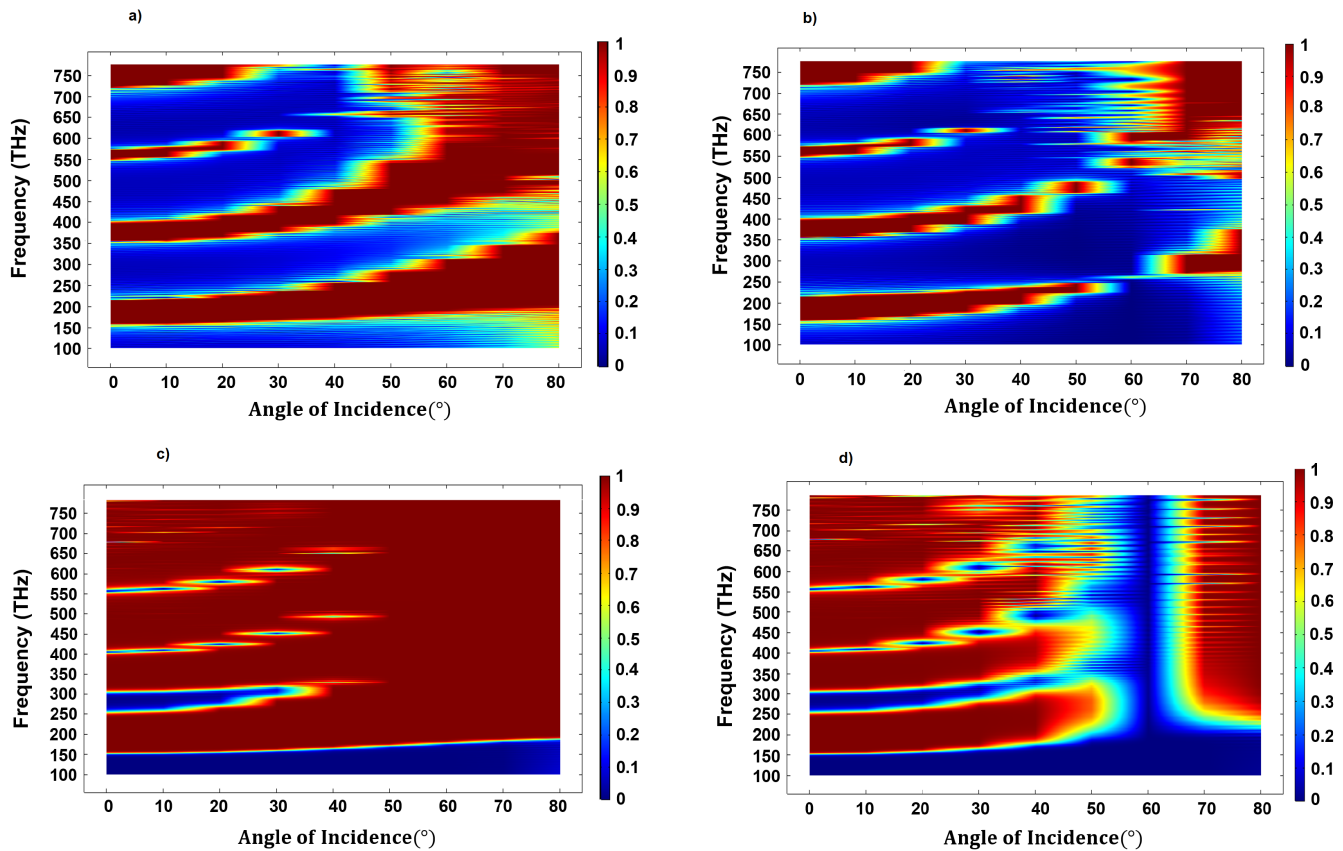


FIG. 6. a) and b) shows the variation reflection spectrum for TE and TM polarization respectively in a normal DBR ($\Lambda = 400 \text{ nm}$ and $d_1 = d_2$) as a function of angle of incidence. c) and d) shows the reflection spectrum for TE and TM polarization respectively in C-DBR as a function of angle of incidence. The C-DBR parameters are $\delta = 10 \text{ nm}$ and $d_1 = 10 \text{ nm}$. All the cases, total number of units is $N = 39$

case of TM polarization in C-DBR and narrow transmission bands. However, Fig. 6(d) exhibits a sharp transmission resonance at the Brewster's angle ($\approx 60^\circ$). The PBGs tend to merge thereafter ($\geq 65^\circ$) giving rise to a broad high reflection band. A comparison between Figs. 6(c) and (d) reveals that the C-DBR could be employed as a broadband ($\approx 150 - 750 \text{ THz}$) polarization filter for $\approx 60^\circ$ AOI. The Brewster's effect is, however, negligible in case of ICT-DBR which is a consequence of monotonic change in intra-cell tilt angle. This leads to a different Brewster's angle in each unit cell for different AOI which reduces the cumulative effect of high-transmission for TM polarization.

III. CONCLUSION

In conclusion, we present an approach to understand the propagation characteristics of modes in a DBR using general techniques adopted in a wide variety of systems exhibiting $SU(2)$ dynamical symmetry. The coupled-mode equations describing the forward and backward

propagating modes in a DBR could be represented in the form of a single *optical* Bloch-equation where the evolution of state-vector depicts the dynamical behaviour of the wave propagation. This provides a platform to draw an analogy with a *two-level* atomic system and consequently, adopt a formalism for adiabatic evolution in DBR based configurations. In order to realize conditions imposed by adiabatic constraints, a few DBR designs namely, ICT-DBR and C-DBR have been investigated in detail. The DBR variants exhibit enhancement of PBG along with varying degree of suppression of sharp transmission resonances in the reflection spectrum. The impact of alteration in physical parameters of the DBR is explored in detail. It is worth pointing out that the C-DBR configuration involves a discernible longitudinal variation in mode-coupling coefficient κ in addition to the sweep in $\Delta\beta$ (or Δk). Conventionally, such adiabatic process have a close resemblance with the *Allen-Eberly* scheme defined in the context of population-transfer in *two-level* atomic systems[19]. Novel DBR designs could further be explored which satisfy the adiabatic constraints. An interesting extension of this proposal

would be to investigate the evolution of *geometric*-phase in such DBR configurations and the possibility to control the backscattered (reflection) phase through suitable DBR design. This promises to provide a unique and flexible platform for tailoring the spatial features of

an optical beam using adiabatic DBR configurations. Nevertheless, a natural extension of this proposal would be to explore the viability of this formalism in *two*- and *three*-dimensional photonic crystals.

-
- [1] E. Yablonovitch, Phys. Rev. Lett. **58**, 2059 (1987).
- [2] R. Sapienza, P. Costantino, D. Wiersma, M. Ghulinyan, C. Oton, and L. Pavesi, Phys. Rev. Lett. **91**, 263902 (2004).
- [3] J. D. Joannopoulos, S. G. Johnson, J. N. Winn, and R. D. Meade, *Photonic Crystals Molding the Flow of Light*, 2nd ed. (Princeton University Press, 2008).
- [4] P. Yeh, A. Yariv, and C.-S. Hong, J. Opt. Soc. Am. **67**, 423 (1977).
- [5] A. Yariv and P. Yeh, *Photonics Optical Electronics in Modern Communications*, 6th ed. (Oxford University Press, 2007).
- [6] M. Kaliteevski, I. Iorsh, S. Brand, R. A. Abram, J. M. Chamberlain, A. V. Kavokin, and I. A. Shelykh, Phys. Rev. B **76**, 165415 (2007).
- [7] M. K. Shukla and R. Das, Opt. Lett. **43**, 362 (2018).
- [8] K. Mitsuteru, O. Kazuaki, and T. Miyamoto, J. Appl. Phys. **50**, 1222 (1979).
- [9] L. Maigyte and K. Staliunas, Appl. Phys. Rev. **2**, 011102 (2015).
- [10] Y. Shen, J. Fu, and G. Yu, Phys. Lett. A **43**, 3801 (2011).
- [11] K.-y. Xu, X. Zheng, C.-l. Li, and W.-l. She, Phys. Rev. E **71**, 066604 (2005).
- [12] B. West and A. Helmy, J. Opt. Soc. Am. B **23** (2006), 10.1364/JOSAB.23.001207.
- [13] E. Simova and I. Golub, Opt. Express **11**, 3425 (2004).
- [14] A. Mizrahi and L. Schächter, Phys. Rev. E **70**, 016505 (2004).
- [15] C. Wächter, F. Lederer, L. Leine, U. Trutschel, and M. Mann, J. Appl. Phys. **71**, 3688 (1992).
- [16] I. V. Iorsh, P. A. Belov, A. A. Zharov, I. V. Shadrivov, and Y. S. Kivshar, Phys. Rev. A **86**, 023819 (2012).
- [17] B. Afinogenov, A. Popkova, V. Bessonov, B. Lukyanchuk, and A. Fedyanin, Phys. Rev. B **97** (2018), 10.1103/PhysRevB.97.115438.
- [18] C. Denz, S. Flach, and Y. S. Kivshar, *Nonlinearities in Periodic Structures and Metamaterials* (Springer, 2008).
- [19] L. Allen and J. H. Eberly, *Optical Resonance and Two-Level Atoms* (Dover Publications, 1987).
- [20] H. Suchowski, D. Oron, A. Arie, and Y. Silberberg, Phys. Rev. A **78**, 063821 (2008).
- [21] A. Karnieli and A. Arie, Opt. Express **26**, 4920 (2018).
- [22] A. Karnieli and A. Arie, Phys. Rev. Lett. **120** (2018), 10.1103/PhysRevLett.120.053901.
- [23] Y. Li, O. Yesharim, I. Hurvitz, A. Karnieli, S. Fu, G. Porat, and A. Arie, Phys. Rev. A **101**, 033807 (2020).
- [24] A. Yariv and P. Yeh, *Optical Waves in Crystals Propagation and Control of Laser Radiation* (New York Wiley, 1984).
- [25] R. Garg and K. Thyagarajan, Opt. Fiber Tech. **19**, 148 (2013).
- [26] K. Thyagarajan and R. Garg Gupta, J. Mod. Opt. **63**, 1 (2016).
- [27] R. Feynman, F. Vernon, and R. Hellwarth, J. Appl. Phys. **28**, 49 (1957).
- [28] E. Bahar, X. Ding, A. Dahan, H. Suchowski, and J. Moses, Opt. Express **26**, 25582 (2018).
- [29] A. Markov, A. Mazhorova, H. Breitenborn, A. Bruhacs, M. Clerici, D. Modotto, O. Jedrkiewicz, P. di Trapani, A. Major, F. Vidal, and R. Morandotti, Opt. Express **26**, 4448 (2018).
- [30] O. Yaakobi, L. Caspani, M. Clerici, F. Vidal, and R. Morandotti, Opt. Express **21**, 1623 (2013).